Modeling the Length of Distal Radioulnar Ligaments

Liz Marai

April 2001

Abstract

The distal radioulnar ligaments are essential contributors to wrist joint stability. We present a CT-based model for ligament displacement, in which ligaments are approximated by shortest paths in a 3D space with bone obstacles. This first model allows for the study of distal ligaments biomechanics *in vivo* and non-invasively. We show that our simplified model gives surprising insight into distal ligament and wrist biomechanics. We apply our ligament model to 6 patients with recalcitrant limitation of forearm rotation and present results. As byproducts, a better bone surface reconstruction via manifolds is achieved, and a novel method for automated alignment/comparison of the same bone across different patients is proposed.

1   Introduction

The distal radioulnar joint (DRUJ) is the distal joint in the complex anatomy of the forearm that allows the wrist and hand to be rotated from pronation to supination (see Figure 1). This movement provides torque to the wrist ('wraestan' means to twist), allowing transfer of rotational force to the grasping hand. Therefore, a clear understanding of the DRUJ biomechanics is important to an understanding of the function of the forearm and wrist.

Wrist rotation via the distal joint is the result of a complex interplay between the bones (radius and ulna) and the soft tissues of the entire forearm. Motion between the radius and ulna is, in fact, more complicated than the simple rotation of the radius around the fixed ulna, shown in Figure 1; there is evidence that translation, axial motion, and counter rotation of the ulna are also present [1].

DRUJ stability during the forearm twist is provided by the contour of the bone extremities, the surrounding ligaments (tough/elastic bands of tissue connecting bone extremities together), and the crossing muscles. As the two radii of the radius and ulna joint surfaces are significantly different, the joint surface contact is optimal only in the neutral forearm position [2]. The contribution
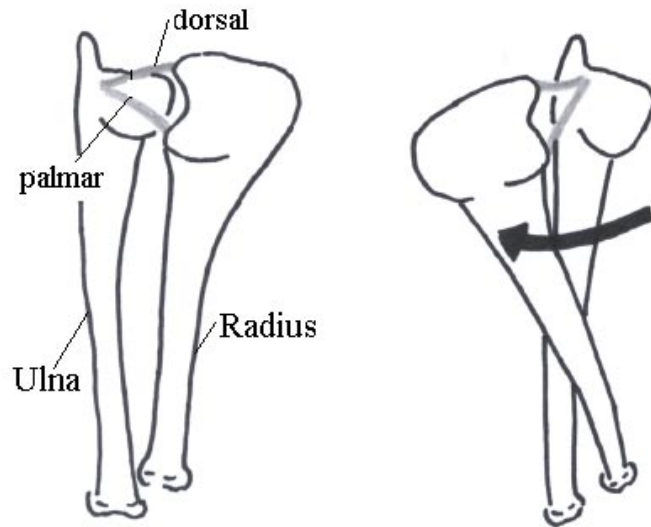
Figure 1: Right forearm (wrist up) rotation: a) supination (palm facing viewer); b) pronation - radius crossed (back of the hand facing viewer). The palmar and dorsal radioulnar ligaments are shown in gray.

of the bone contours to joint stability decreases with increasing pronation or supination, because the contact area gradually diminishes.

180° of motion with intact stability is still possible thanks to the dorsal and palmar distal radioulnar ligaments - two stabilizing ligaments which anchor the swinging radius to the ulna. The dorsal and palmar radioulnar ligaments (shown in gray in Figure 1) have their origin in the dorsal and palmar corners of the distal radius and converge toward the base of the styloid process of the ulna.

Understanding the biomechanics of the distal radioulnar ligaments is important for a number of reasons. Both trauma of the wrist and degenerative attenuations result in ligament damage and instability of the DRUJ. Post traumatic limitation of forearm rotation is common; this limitation is often accompanied by pain and refractory to extensive rehabilitation. Repairing or augmenting distal radioulnar ligaments to recover joint stability is receiving increased recognition as a treatment method, but we must know how these ligaments move during pronosupination of the forearm in order to identify the ligament which requires reconstruction. Early reconstruction of the structures stabilizing the joint can also prevent the development of permanent joint damage, since prolonged joint instability can lead to osteoarthritis [3]. Safe immobilization after trauma is

also a challenging problem: following an injury in which a ligament has been ruptured, the forearm should be immobilized for the necessary healing period with the repaired ligament in a relaxed state; this position cannot be determined without knowledge of the biomechanics of the ligament.

Unfortunately, various medical authorities hold contrary opinions (based on anatomical and/or invasive clinical studies) regarding distal radioulnar ligament motion during DRUJ pronation and supination ("the dorsal distal ligament is taut in pronation" [2] versus "the dorsal distal ligament is relaxed in pronation" [4, 3], for example), thus implying opposite techniques and treatment guidelines for reconstruction of the unstable distal joint. A non-invasive *in vivo* study of the DRUJ biomechanics is still missing. The present study is a first step towards filling in this gap.

Ligament biomechanics are complex. Ideally they should be studied dynamically, with all factors considered. In such a study, intrinsic factors of ligaments such as fiber orientation, composition, insertion and origin would be considered, as would extrinsic factors such as muscle pull, compression of the joint, and position of the adjacent bones. At present, the realization of this ideal goal seems distant. Current *in vivo* imaging techniques include computed tomography (CT) and magnetic resonance imaging (MRI). CT is, in general, preferred when investigating wrist dysfunctions, since it is less expensive than MRI, and, more important, it reveals more clearly the structure (and possible defects) of the bones in the wrist. Unfortunately, wrist ligaments are at the same time not dense enough to show on CT scans, and difficult to identify in MRI scans.

With these thoughts in mind, we present a CT-based method for modeling the changes in length of the distal radioulnar ligaments with forearm pronation/ supination. We model the distal ligaments as minimum paths running from origin to their respective anchor points; these paths are constrained to avoid bone penetration. We are primarily interested in: 1)measuring the relative displacement the distal ligaments undergo during pronation and supination (and less in measuring the ligament laxity or tautness); and 2)approximating *in vivo* the motion of the distal radioulnar ligaments during pronosupination. Our model makes use of the following simplifying assumptions:

1. other tissues in the wrist exercise negligible forces;

2. ligaments are under some tension at any given time;

3. bones have no snags.

In particular we apply our method to data (12 CT scanned wrists) coming from 6 patients suffering from posttraumatic (malunited distal fracture of the radius) limitation of forearm rotation. We show that even the simplified length model we propose provides unexpected insight into the biomechanics of the forearm, and, more importantly, it reveals significant and interesting differences between normal and injured DRUJ kinematics.

2   Related Work

The distal radioulnar ligaments enjoy a lot of attention in the medical world. Studies are performed in general on fresh frozen cadaver healthy wrists [2, 3, 4], and give thus little and unreliable information about wrist kinematics and none about wrist pathologies. A clinical *in vivo* study involving surgery was performed by Kleinman et al. in 1998 [1]. No *in vivo* non-invasive studies of the distal radioulnar ligaments are known.

Searching for shortest paths in spaces with obstacles is a classical problem in robotics. Solutions to the problems are based on computational geometry methods [7, 5, 6, 8], differential geometry and hybrid techniques [10, 11], as well as graph search based algorithms [9]. A survey of the substantial literature on various cases of the shortest path problem can be found in [12].

Our shortest path approach uses an implicit representation of the bone, a "scalar distance field". Regularly sampled distance fields have been used in robotics for path planning [20, 21], swept volumes [22], volume rendering [19], offset surfaces [23, 24], and morphing [25, 24]. Level sets [26, 27] have been both used to generate distance fields and generated from distance fields.

Several approaches for modeling joint surfaces are known. Thin-plate splines [13], B-splines [14, 15], and piecewise patches [16] are examples. These methods suffer from problems such as lack of generality, lack of C^2 continuity, and difficulty in enforcing boundary constraints. Our model for bone surfaces is based on manifolds [18].

3   Methods

We are using data collected from 6 patients of varying age. All subjects have experienced dorsal distal fractures of the radius in one forearm. All patients have restored osseous anatomy after trauma, but have failed to regain prono-supination (full forearm rotation) after maximal rehabilitation.

Our method pipeline is depicted in Figure 2. At the front end of the pipeline is the data acquired from the patients. Both forearms (healthy and injured) of a given patient are axially scanned using computed tomography (Hispeed Advantage, GE Medical Systems). The scans are repeated for 6 to 7 pronosupination positions. Volume images (stacks of slices for each scan) are obtained with the voxel dimensions of 0.234x0.234x1 mm^3. Points corresponding to the bone cortex are extracted from each raw CT slice. These points are later assigned to the bone from which they originated, via custom software and substantial user interaction. The result of this segmentation procedure is a cloud of 3D points for each bone. The rigid transformation which takes each bone from the initial neutral position to the current scan position is recovered using moments of inertia, as described in [29]. All forearms are converted to right forearms, for ease of comparison.
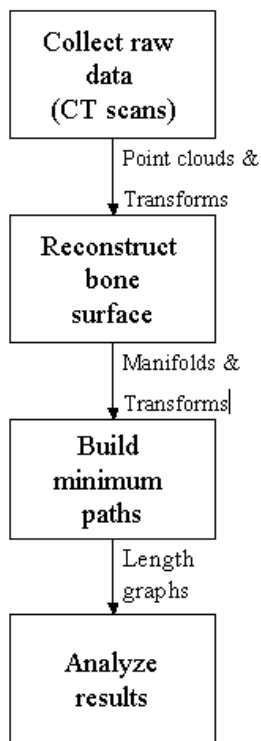
Figure 2: Method pipeline

From a cloud of points we reconstruct the bone surface; the result is a continuous, locally parameterized representation of the bone cortex. On this continuous representation we identify the insertion and origin points of a given ligament, we run an algorithm for minimum paths, and we evaluate the length of the resulted path. We repeat the minimum path computation over the different pronosupination positions, for both forearms of a given patient. For each patient we compare the results obtained for the healthy and the injured forearm. Since the location of the insertion/origin points is not 100% accurate, we displace these points on the surface of the bone and check the stability of our minimum paths.

Since the focus of this study are ligament lengths, we proceed by presenting first the minimum length path algorithm (section 3.1), and then the bone surface reconstruction module (section 3.2).
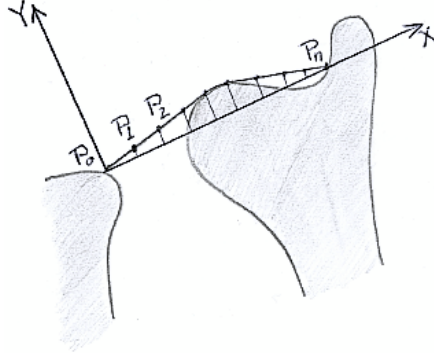
Figure 3: Shortest path - 2D case

3.1 Minimum Paths

Minimum/shortest paths in 3D with stationary obstacles are a classical problem. Solutions to this problem are based on computational geometry methods, differential geometry and hybrid techniques, as well as graph search-based algorithms, depending to some extent on the type of the obstacles (polyhedral or continuous surfaces). Although a polyhedral approximation of our bone surface can be easily generated (and it is generated, for rendering purposes), we compute the shortest paths using the continuous representation. Standard computational procedures to obtain minimum length paths in spaces with continuous surfaces are more accurate than the graph approximation algorithms, but they yield paths that are only locally optimal. We need a good initial guess to increase the likelihood of convergence to the globally optimal path, but this initial guess is rather easy to find in the case of ligaments and bones, as we will show a little later. Our shortest paths algorithm therefore uses a numerical optimization approach.

We begin the description of the algorithm with a simplified example in 2D, depicted in Figure 3. In this example, we are required to find a shortest path from the insertion point p_0 to the point p_n, so that the path does not penetrate the 2D bone-obstacle on the right.

We start by attaching a local 2D coordinate system to the bones, so that the origin of the system is in p_0, and the X axis is the line defined by p_0 and p_n.

We choose $n-1$ additional points (equally spaced) on the p_0p_n segment. On our smooth bone representation we define a signed distance function as follows: the function is zero on the surface of the bone, positive outside, and negative inside. At each point where it is non-zero, the function will measure the distance from the point to the nearest surface point.

We reformulate our problem in the following terms: "find the coordinates of the $n-1$ points so that the length of the path $p_0p_1p_2...p_n$ is minimum and
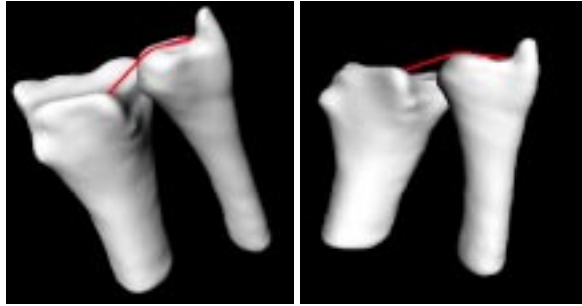
Figure 4: Generated shortest paths (shown in red)

$distance(p_i, bone) \geq 0$, for $i = 1, ..n - 1$". If we fix the x coordinates of the points so that they are initially equally spaced on the $p_0 p_n$ segment, our problem amounts to minimizing the Euclidean length of the path over the y_i coordinates of the points.

The formulation described above can be easily extended to 3D, where we optimize over both the y and the z coordinates of the points. The problem we are solving is actually more complicated - there are two obstacles in our scene, but since these obstacles appear always in a sequence, the extension of the algorithm is straightforward.

We pass the optimization problem to a numerical solver (NAG Fortran Library Routine - E04UCF [28]) which makes use of a sequential quadratic programming method. Given the structure of our search space and the smoothness of the distance function the optimization converges to a minimum. In some cases - given the geometry of the two forearm bones - this minimum corresponds to the straight line between p_0 and p_n. When the straight line actually penetrates the bone, the question of a local/global minimum arises. A costly general solution to avoiding local minima would be to run first an approximation graph algorithm on a coarse tessellation of the bone. The preliminary solution obtained would indicate the area of interest corresponding to the global minimum; we could pass this coarse solution as an input to the numerical optimization procedure. This solution would require, however, building a massive visibility graph. Since in our case the area of the global minimum is obviously the head of the bones (which in general is smooth) we prefer to use repeated restarts (with different initial start solutions) of the optimization procedure. We are using three different start solutions:

1. points on the straight $p_0 p_n$ line;

2. points on an elevated line;

3. points generated by the procedure in the previous pronosupination position.

We have found that the optimization procedure converges to the same solution in all three cases (with an increasing computational effort from case 1 to
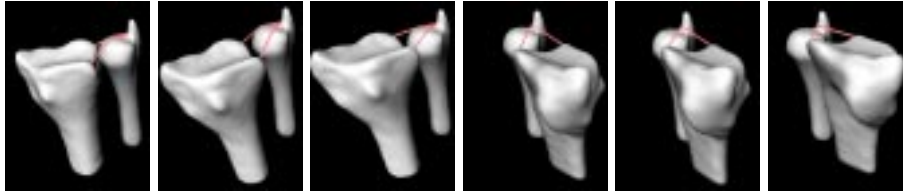
7

Figure 5: Shortest paths (sequence from pronation to supination)
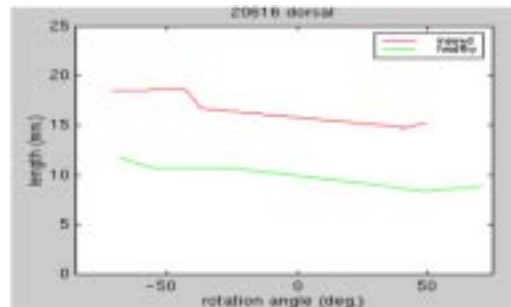

Figure 6: Length of the dorsal ligament shown in Figure 5 (red). The corresponding length graph of the matching uninjured forearm is shown in green. The X axis: rotation angles in helical axis of motion coordinates (deg.); the Y axis: ligament displacement (mm)

case 2 to case 3).

We choose the number of points n to be the smallest number for which the length of the path stabilizes. This number is usually in the [30; 60] range. Figure 4 shows two shortest paths generated with our algorithm.

Repeating the shortest path procedure over 6 different pronosupination positions yields a sequence like the one shown in Figure 5; the dorsal radioulnar ligament length graph corresponding to this sequence is shown in red in Figure 6. We show in green the corresponding length graph generated for the matching healthy forearm - note the significant difference between the two plots.

3.2   Bone Surface Reconstruction

We recover bone surfaces from CT scans by fitting a smooth, locally parameterized model to the non-uniform set of data points generated by the scanner. The parameterized model we use is based on *manifolds* (for a presentation of manifolds see [18]). There are several advantages to using a manifold model for representing bone surfaces. First, CT scans produce sample points which are densely packed along relatively widely spaced contours. Manifolds provide

Figure 7: Point cloud representing a ulna bone (white) and the canonical ulna model (pink).

a natural method for doing a coarser to finer fit to such a data point set. The layered-fitting method helps with the sparse data problem since the coarser fit can be used in areas with few sample points and the finer fit applied only where needed [17]. Second, manifolds are locally parameterized and highly deformable, which means they can easily fit across the same bone for multiple people and thus allow for consistent comparisons. Lastly, manifolds make possible the definition of what we call 'distance fields'. A distance field is a scalar field surrounding a closed surface, which specifies the signed minimum distance from a point inside the field to the surface. This field can be stored as a sampled data set, much like a CT data set, and can be used for geometric operations such as distance calculation, collision detection, or level surface generation.

One drawback to the manifold approach is that the initial, unfitted manifold must be constructed by hand. We ameliorate the cost of this procedure by reusing the manifolds from one patient to another, as we further describe; thus only one model (the 'canonical model') per bone type needs to be constructed by hand. There are two problems, however, in reusing manifolds across patients. First, the manifold needs to be aligned with the data set prior to deforming it to fit the data. Unfortunately, bones from different patients are scanned in different positions and orientations. Second, forearm bones are not scanned to the same length: some are scanned almost up to the elbow, some just a little above the wrist. This poses problems to the manifold model, which was built with extra length: assuming we align the manifold with the data set, parts of the manifold model will have no data points to fit to. We address these problems as follows: we first align the manifold model to the new data set, then chop the manifold to match the length of the bone which generated the data set, and finally deform the chopped manifold so that it fits the data set. We proceed by describing the automated alignment procedure.

As shown in Figure 7, our problem amounts to finding the rigid transform which would align the canonical manifold surface (shown in pink) to the data set (shown in white). Using moments of inertia (the standard method) is unfortu-

nately not an option, since our datasets are non-uniform [29]. Manual alignment requires unacceptably extensive user interaction. The third option (and the one we choose) is to use an error-to-surface minimization technique.

Our alignment method proceeds in three steps: 1)approximate the alignment translation based on the center of the bounding boxes of the canonical model and of the point cloud; 2)find the rotation axis and angle which minimizes the squared error from the points in the data set to the canonical surface; 3)refine the translation and the rotation found in the previous steps so that the squared error-to-surface is minimum.

We use a quasi-Newton optimization algorithm (NAG Fortran Library Routine - E04JAF [30] for steps 2 and 3). This algorithm yields a local minimum, therefore for step 2) we use repeated restarts with different initial values of the normalized rotation axis and of the rotation angle; we are currently using 14 different orientations for the initial rotation axis (uniformly distributed on the surface of the unit sphere), and 4 different values for the initial rotation angle. We have applied the alignment procedure described to both carpal bones (the eight small bones in the wrist) and to forearm bones. The algorithm needs a slight adjustment for forearm bones. Since such bones may be shorter than their corresponding canonical model, we replace the initial bounding box translation described in step 1) with the following procedure: find the long axis of the bone / canonical model, then compute the initial translation based on the distance along this long axis from the center of the bounding box to the head of the model. We should mention that, although the automated alignment procedure worked fine on more than 50 bone data sets, its limitations remain still to be explored.

Once the alignment is completed, we chop the manifold model and regenerate its bottom so that it matches the length of the bone (this step is not necessary in the case of the forearm bones), and then deform the canonical model so that it fits the data set. A full decription of the fitting procedure can be found in [17]. Figure 8 shows results obtained with our bone surface reconstruction method (the bone data sets are meshified for visualization purposes).

4   Results

Figure 9 and Figure 10 show ligament length graphs obtained for our set of 6 patients. In each graph we are comparing the length of a healthy wrist ligament (green) to the one of the matching injured wrist ligament (columns correspond to patients).

A first observation is that in all normal forearms the dorsal ligament seems to be taut in pronation and relaxed in supination, confirming the findings of Acosta et al. [3] and Schuind et al. [4], and infirming the observations of Ekenstam [2]. According to Acosta and Schuind, the normal palmar ligament should be taut in supination and relaxed in pronation. We do not find enough evidence in our
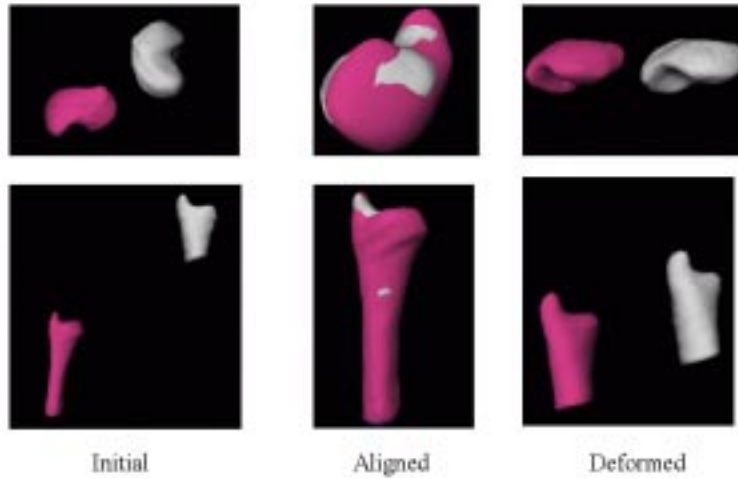
Figure 8: Results of the bone surface reconstruction method. Top row: carpal bone, bottom row: forearm bone. The bone data sets are meshified for visualization purposes only (bones are shown in white and the manifold models in pink).

measurements to support this theory.

A second and more important finding refers to the injured forearms. A larger or smaller difference in the length of the dorsal ligament (top row) between the injured and the healthy forearm appears in all 6 patients. No significant difference appears in the case of the palmar ligament (bottom row). Given that all of our patients suffered dorsal fractures of the radius, this discrepancy does not come as a surprise: we expect more damage to appear on the same side as the original fracture. We are questioning, however, the reliability of our observation: the difference in length might be due to the particular placement of the ligament anchor points.

To eliminate the doubt we perform an insertion point study on the pair of forearms which generated the smallest length difference (middle column, Figure 9). We perturb the location of the insertion and origin points within a 4mm diameter area and rerun the shortest path algorithm. The results we obtain (shown in Figure 11) are consistent with our previous findings: the difference in the length of the dorsal ligament is preserved.

The shortest paths generated by our approach gave us, however, the most interesting piece of information. Figures 12 and 13 show an entire healthy pronosupination sequence versus the matching injured sequence. We found that, due to the specific geometry of the two forearm bones, in all 6 healthy cases the shortest paths are actually straight lines between the insertion and origin points (as shown in Figure 12). In all 6 injured cases, besides increased distances between the radius and the ulna, we found that the shortest paths stretch over the
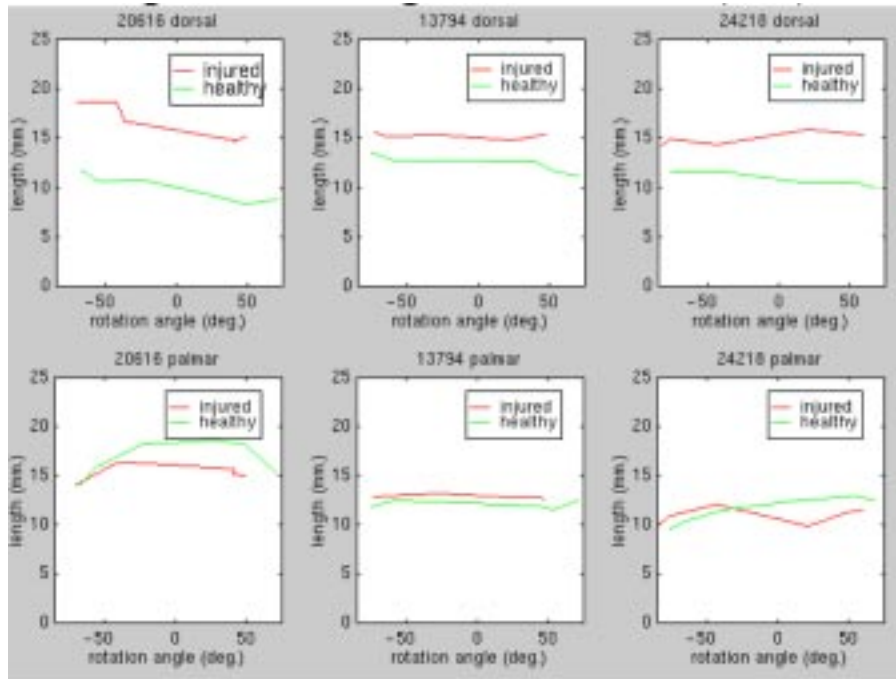
Figure 9: Ligament length graphs. Columns corespond to patients, top row: dorsal radioulnar ligament, bottom row: palmar radioulnar ligament. The X axis measures rotation angles in helical axis of motion coordinates (deg.); the Y axis measures ligament displacement (mm). Note the difference in dorsal ligament length (top row) between healthy and matching injured forearms.

head of the ulna, especially towards pronation (as shown in Figure 13). This seems to indicate a dramatic alteration of normal forearm kinematics.

The most plausible explanation for these findings is that the injured radius has become a little shorter, either during the fracture (a small fragment of bone got displaced) or during the healing process (two parts of the bone fused in an incorrect position). Although this shortening is on the order of millimeters and therefore hard to track down from a raw CT scan, from our visualization it is obvious that it destroys the balance of the DRUJ, with inherent effects on the radioulnar ligaments (thus, the limitation and the pain). Figure 14 highlights the effect of the radius shortening on the contact area between the two bones: the ulna contact area for the injured forearm is systematically below that for the matching healthy forearm, especially toward pronation. This situation could be remedied either by inserting a wedge into the radius on the side with the fracture, or by shortening the ulna bone so that it matches the length of the radius [1].
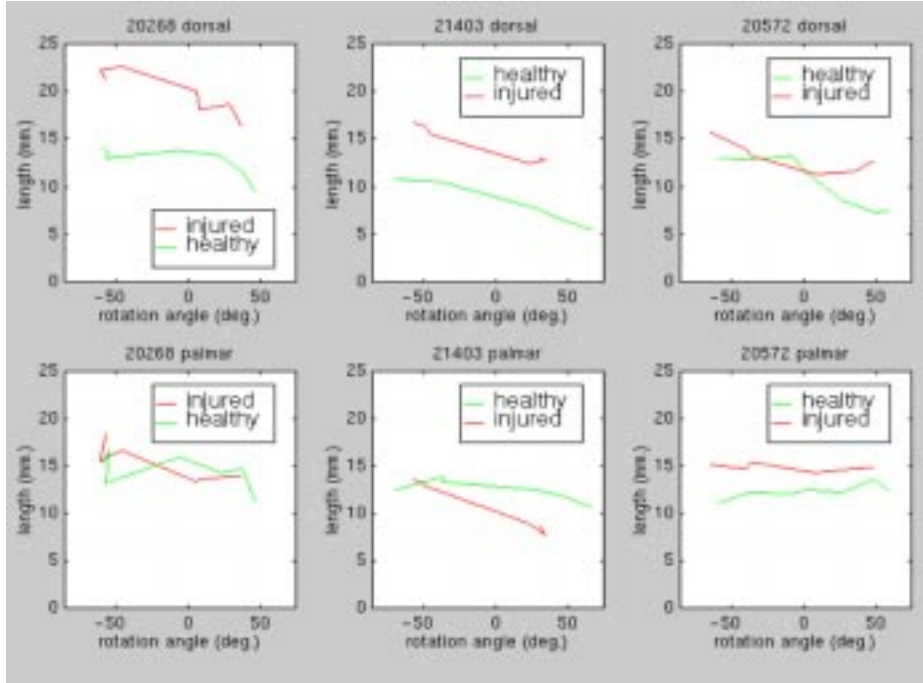
Figure 10: Ligament length graphs (CT scans of poorer quality). Columns correspond to patients, top row: dorsal radioulnar ligament, bottom row: palmar radioulnar ligament. The X axis measures rotation angles in helical axis of motion (HAM) coordinates (deg.); the Y axis measures ligament displacement (mm). Rotation angles in HAM coordinates compensate for the relative motion of the ulna with respect to the humerus, thus they do not come in strictly increasing order from pronation to supination.

5 Conclusion and Future Work

Restoring stability to the DRUJ is crucial for regaining optimal function of the forearm and wrist. To improve the treatment of distal forearm fractures or of wrist joint degenerative attenuations, knowledge about the biomechanics of the distal radioulnar ligaments is essential.

We have demonstrated an *in vivo*, non-invasive technique for modeling the length of the distal radioulnar ligaments. Although simple, this model provides useful insight into the biomechanics of injured and healthy wrists. In the case of 6 patients with post traumatic limitations of forearm rotation, our approach highlighted subtle modifications, otherwise unnoted, in injured wrist kinematics. With the knowledge provided by our study, a surgical approach to this set of patients can be developed.
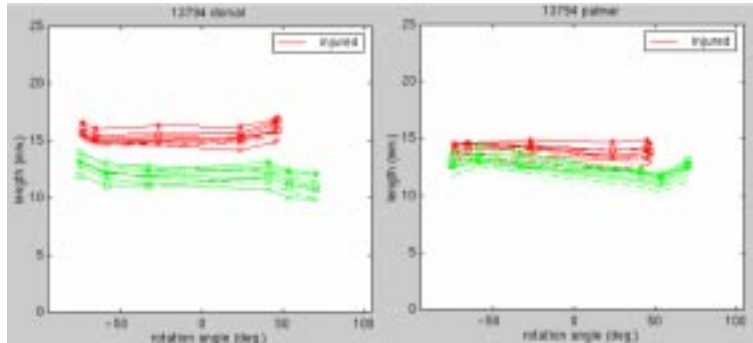
13

Figure 11: Insertion point study: a) dorsal ligament; b) palmar ligament

We hope to apply the current model to other ligaments in the wrist, and explore correlations, if any, between wrist disorders such as effects of rheumathoid arthritis or inter-carpal ligament tear/attenuation and ligament lenghts.

We are interested in exploring the use of the automated alignment routine we developed as a tool for bone registration (registration of the bone surface is used to calculate rigid body kinematic variables). Our alignment method promises good kinematic accuracy and can potentially be used to study the non-invasive, three dimensional *in vivo* kinematics of the wrist and other skeletal joints.

Lastly, we have obtained a good bone surface representation via manifolds. The current approach uses hand-drawn contours extracted from thresholded CT images. In the long run we plan to develop an automated segmentation procedure which would allow us to recover bone surfaces directly from the raw CT data via manifold fitting. This method would allow us to avoid both the introduction of extraneous contour data to the scanned data, and the current massive user interaction.
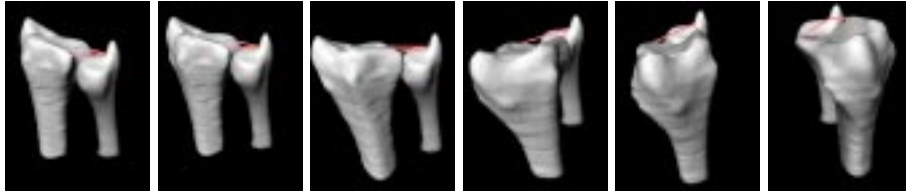
Acknowledgements

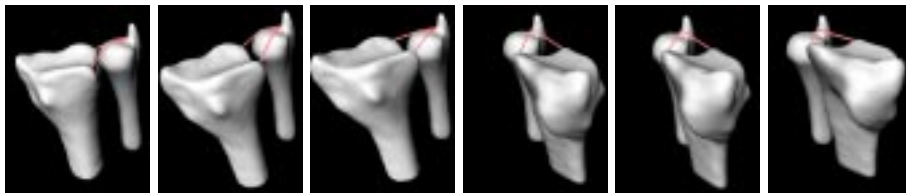Figure 12: Healthy sequence from pronation to supination

Figure 13: Injured sequence from pronation to supination

References

[1] W. Kleinman, T. Graham, "The distal radiolunar joint capsule: clinical anatomy and role on posttraumatic limitation of forearm rotation", *The Journal of Hand Surgery*,Volume 23A, No. 4, pp.588-599, 1998

[2] F. Ekenstam, "Anatomy of the Distal Radioulnar Joint", *Clinical Orthopaedics*, Volume 275, pp.14-18, 1992

[3] R. Acosta, W. Hnat, L.R. Sheker, "Distal radio-ulnar ligament motion during supination and pronation", *The Journal of Hand Surgery (British and European Volume)*, Vol. 18B, pp.502-505, 1993

[4] F. Schuind, K. An, L. Berglund, R. Rey, W. Cooney, R. Linscheid, E. Chao, "The distal radioulnar ligaments: a biomechanical study", *The Journal of Hand Surgery* , Volume 16A, No. 6, pp.1106-1114, 1991

[5] C.H. Papadimitriou, "An Algorithm for Shortest-Path Motion in Three Dimensions", *Information Processing Letters*, Vol. 20, 1985, pp. 259-263

[6] K. Clarkson, "Approximation Algorithms for Shortest Path Motion Planning", *Proc. 19th Annual SIGACT Symposium*, pp.56-65, 1987

[7] M.Scharir, A. Schorr, "On shortest paths in polyhedral spaces", *SIAM J. Comput.*,Vol. 1(15), pp193-215, 1986

[8] A. Baltsan, M. Scharir, "On shortest paths between Two Convex Polyhedra", *JACM*, Vol. 35 (2), pp.267-287, 1988

[9] N. Kiryati, G. Szekely, "Estimating Shortest Paths and Minimal Distance on Digitized Three Dimensional Surfaces", *Pattern Recognition*, Vol.26, pp.1623-1637, 1993

[10] R. Kimmel, N. Kiryati, "Finding Shortest Paths on Surfaces by Fast Global Approximation and Precise Local Refinement", *Int. Journal of Pattern Recognition and Artificial Intelligence*, Vol.10(6), pp.643-656, 1996

[11] J.M. Beck, R.T. Farouki, J.K. Hinds. "Surface Analysis Methods", *IEEE Computer Graphics and Applications*, Vol. 6, pp.18-37, 1986

[12] C. K. Yap, "Algorithmic motion planning" *Advance in Robotics, Volume I*, Lawrence Erlbaum Associates, 1985.

[13] S. K. Boyd, J. L. Ronsky, D. D. Lichti, D. Salkauskas, and M. A. Chapman, "Joint surface modeling with thin-plate splines", *Journal of Biomechanical Engineering*, 121, pp. 525-532, October 1999.

[14] G. A. Ateshian, "A b-spline least-squares surface fitting method for articular surfaces of diarthrodial joints", *ASME Journal of Biomechanical Engineering*, 115, pp. 366-373, 1993.

[15] G. A. Ateshian, "Generating trimmed b-spline models of articular cartilage layers from unordered 3d surface data points", *Proc. ASME Bioengineering Conference*, pp. 217-218, 1995.

[16] P. K. Scherrer and B. M. Hillberry, "Piece-wise mathematical representations of articular surfaces" *Journal of Biomechanics*, 12, pp. 301-311, 1979.

[17] C. Grimm, J.J. Crisco, D.H. Laidlaw, "Fitting locally parametric surfaces to 3D point clouds", submitted to *ASME Journal of Biomechanical Enginnering*

[18] C. Grimm and J. Hughes, "Modeling Surfaces of Arbitrary Topology using Manifolds" *Computer Graphics*, 29(2), July 1995, Proceedings of SIGGRAPH'95

[19] S. Gibson, "Using Distance Maps for smooth surface representation in sampled volumes," *Proc. 1998 IEEE Volume Visualization Symposium*, pp. 23-30, 1998.

[20] R. Kimmel, N. Kiryati and A. Bruckstein, "Multi-valued distance maps for motion planning on surfaces with moving obstacles", *IEEE Trans. on Robotics & Automation,Symposium*, 14, pp. 427-436, 1998.

[21] J. Lengyel, M. Reichert, B. Donald and D. Greenberg, "Real-time robot motion planning using rasterizing computer graphics hardware", *Proc. SIGGRAPH 90*, pp. 327-335, 1990.

[22] W. Schroeder, W. Lorensen, and S. Linthicum, "Implicit modeling of swept surfaces and volumes," *Proc. Visualization '94*, pp. 40-45, 1994.

16

[23] D. Breen, S. Mauch and R. Whitaker, "3D scan conversion of CSG models into distance volumes" *Proc. 1998 IEEE Symposium on Volume Visualization*, pp. 7-14, 1998.

[24] B. Payne and A. Toga, "Distance field manipulation of surface models," *IEEE Computer Graphics and Applications* , pp. 65-71, 1992.

[25] D. Cohen-Or, D. Levin, and A. Solomovici, "Three-dimensional distance field metamorphosis", *ACM Transactions on Graphics*, 1997.

[26] S. Osher and J. Sethian, "Fronts propagating with curvature-dependent speed: algorithms based on Hamilton-Jacobi formulation", *J. Computational Physics*, 79, pp. 12-49, 1988.

[27] J. Sethian, *Level Set Methods: Evolving Interfaces in Geometry, Fluid Mechanics, Computer Vision, and Material Science* , Cambridge University Press, 1996.

[28] "E04UCF - NAG Fortran Library Routine Document", *http://www.nag.co.uk/numeric/fl/manual/html/e04%5Ffl19.html*

[29] C. P. Neu, R. D. McGovern, J. J. Crisco, "Kinematic accuracy of three surface registration methods in a three-dimensional wrist bone study", *Journal of Biomechanical Engineering (Volume 122, 2000)*,pp. 1-6

[30] "E04JAF - NAG Fortran Library Routine Document", *http://www.nag.co.uk/numeric/fffg/ff01/e/e04jaf.html*
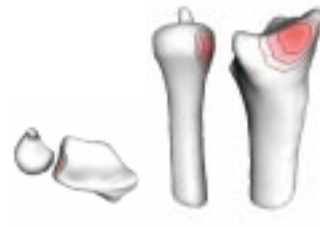
17
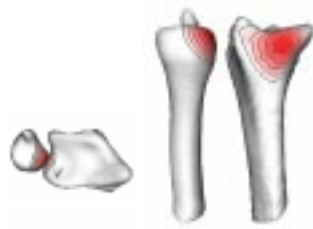
(a) healthy:+70.9

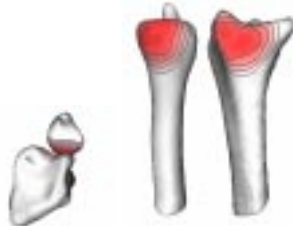(b) injured:+49.2

(c) healthy:+48.9
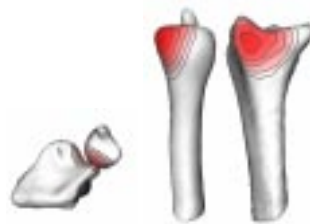
(d) injured:+39.8

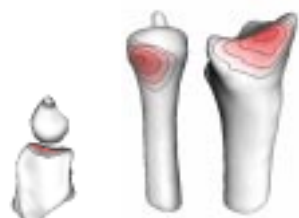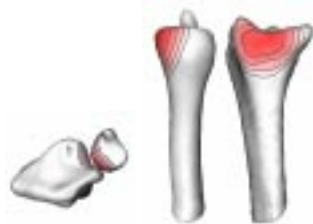(e) healthy:+27.9

(f) injured:+41.7

(g) healthy:-24.7

(h) injured:-37.1

(i) healthy:-54.78

(j) injured:-42.8

(k) healthy:-67.9

(l) injured:-70.7

Figure 14: Top and rotated side views of a healthy radioulnar joint at 6 angular positions, versus top and rotated side views of the matching injured radioulnar joint at 6 angular positions. The angles go from supination (radius straight) to pronation (radius crossed over). Bones are colored according to the distance between them (the closer, the more intense the color). Note the shift in the location of the contact areas between the healthy and the injured forearm.